Some Implications of Ekman Layer Dynamics for Cross-Shelf Exchange in the Amundsen Sea

A. K. WÅHLIN

Department of Earth Sciences, University of Gothenburg, Gothenburg, Sweden

R. D. MUENCH

Earth and Space Research, Seattle

L. ARNEBORG AND G. BJÖRK

Department of Earth Sciences, University of Gothenburg, Gothenburg, Sweden

H. K. HA AND S. H. LEE

Korea Polar Research Institute, Incheon, South Korea

H. ALSÉN

Department of Earth Sciences, University of Gothenburg, Gothenburg, Sweden

(Manuscript received 25 February 2011, in final form 30 January 2012)

ABSTRACT

The exchange of warm, salty seawater across the continental shelves off West Antarctica leads to subsurface glacial melting at the interface between the ocean and the West Antarctic Ice Sheet. One mechanism that contributes to the cross-shelf transport is Ekman transport induced by along-slope currents over the slope and shelf break. An investigation of this process is applied to the Amundsen Sea shelfbreak region, using recently acquired and historical field data to guide the analyses. Along-slope currents were observed at transects across the eastern and western reaches of the Amundsen slope. Currents in the east flowed eastward, and currents farther west flowed westward. Under the eastward-flowing currents, hydrographic isolines sloped upward paralleling the seabed. In this layer, declining buoyancy forces rather than friction were bringing the velocity to zero at the seabed. The basin water in the eastern part of the shelf was dominated by water originating from 800–1000-m depth off shelf, suggesting that transport of such water across the shelf frequently occurs. The authors show that arrested Ekman layers mechanism can supply deep water to the shelf break in the eastern section, where it has access to the shelf. Because no unmodified off-shelf water was found on the shelf in the western part, bottom layer Ekman transport does not appear a likely mechanism for delivery of warm deep water to the western shelf area. Warming of the warm bottom water was most pronounced on the western shelf, where the deep-water temperature increased by 0.6°C during the past decade.

1. Introduction

The broad continental shelf seas off West Antarctica—the Bellingshausen, Amundsen, and Ross Seas—are characterized by cross-shelf exchange of offshore Circumpolar Deep Water (CDW) and shelf water modified through exchanges with the atmosphere and with subsurface glacial ice. The region is typified by ocean–ice sheet interactions with the West Antarctic Ice Sheet that impact both local ecosystems and global climate. Research on the Bellingshausen Sea, at the eastern end of the region, has focused on decadal change, shelf circulation, and the marine ecosystem in the west Antarctic Peninsula (WAP) region (e.g., Hofmann et al. 2004; Klinck et al. 2004). Research on the Ross Sea shelf slope, at the western part

Corresponding author address: A. K. Wåhlin, Department of Earth Sciences, University of Gothenburg, Box 460, Gothenburg 401 30, Sweden.
E-mail: awahlin@gu.se

DOI: 10.1175/JPO-D-11-041.1

of the region, has focused on the impacts of shelfbreak dynamics on cross-shelf transport as it impacts the rate of formation of Antarctic Bottom Water (AABW) on the Ross Sea shelf (e.g., Gordon et al. 2004, 2009; Orsi and Wiederwohl 2009). More recently, interest has focused on the Amundsen Sea, which is situated between the Bellingshausen and Ross Seas. The Amundsen Sea is of interest because it appears at present to be a primary site for accelerated melting of a portion of the West Antarctic Ice Sheet, a situation having implications for global sea level rise (e.g., Rignot 1998; Rignot and Jacobs 2002; Shepherd et al. 2004; Jenkins et al. 2010; Jacobs et al. 2011).

If it is assumed that physical forcing at the shelf break and over the continental slope exerts a primary control over the cross-shelf transport in the western Antarctic, then some likely processes can be identified for this forcing. Perhaps the simplest is through impingement and flow of the Antarctic Circumpolar Current (ACC) onto the shelf in regions where the slope curves cyclonically into the current path and intrusions of ACC water flow onto the shelf via topographic depressions. The resulting regime, which lacks a shelfbreak frontal system and shows continuous water properties from the deep ocean well onto the shelf, typifies the central coast of the WAP (e.g., Klinck et al. 2004; Klinck and Dinniman 2010). In contrast, a well-defined frontal structure dominates the shelf break and upper slope farther west in the Ross Sea (Gordon et al. 2009; Orsi and Wiederwohl 2009). In this second regime, cross-shelf transport consists primarily of a dense outflow of AABW and a compensating on-shelf flow of warmer offshore waters. Dynamic instabilities either in concentrated shelfbreak currents, as in the Ross Sea or Filchner-Ronne margins (Foldvik et al. 2004) or in association with the ACC in regions where it runs close to or along the slope (Klinck et al. 2004; Beardsley et al. 2004; Dinniman and Klinck 2004) might contribute to cross-slope transport. Similarly, pumping of water across the shelf break might occur in response to migrating weather systems (Thoma et al. 2008; Klinck and Dinniman 2010). The present work focuses on cross-shelf Ekman transport in the frictional boundary layer (e.g., Trowbridge and Lentz 1991; MacCready and Rhines 1991; MacCready and Rhines 1993; Garrett et al. 1993; Wåhlin and Walin 2001).

The Amundsen Sea falls between the two shelf types characterized by the WAP and Ross Sea slopes. It has no well-defined on-shelf flow of oceanic water from the ACC. Nor is there sufficient water mass modification on the shelf to generate dense outflows and a corresponding sharply defined frontal and current system overlying the shelf break and upper slope. The melting of the Pine Island Glacier requires a flow of oceanic heat from the shelf break to Pine Island Bay. Such a flow of warm ocean water has been observed in one of the deep troughs crosscutting the continental shelf to the Pine Island Bay (Walker et al. 2007) and to the western Amundsen shelf (Wåhlin et al. 2010). We examine the Ekman mechanism as a potential source for this flow in the frictional transport below along-slope current filaments associated with the ACC.

A presumed along-slope forcing by the ACC can be expected to vary from east to west along the Amundsen Sea in response to proximity of the ACC to the shelf break. Figure 1a shows a sketch of the ACC and the Ross gyre in the Amundsen Sea, as outlined in Orsi et al. (1995). The path of the ACC turns southward as it flows east, the southeastward branch of the Ross Sea gyre and the ACC presumably bifurcating in the offshore region between the Ross and Amundsen Seas. The ACC approaches the continental slope near the central Amundsen Sea and follows it eastward into the Bellingshausen Sea (Orsi et al. 1995). However, measurements of the ACC in the proximity of the Amundsen shelf are sparse, and the bifurcation point is poorly defined.

Here, field results are presented that define slope currents and hydrographic structure along transects in the eastern and western Amundsen Sea (Fig. 1). The dynamics of bottom Ekman transports forced by these slope current conditions are investigated using analytical techniques, and implications for the water mass characteristics in the broad shelf shoreward of the shelf break are discussed.

2. Observed conditions

a. Hydrographic characteristics and time changes

The Amundsen shelf extends ~300 km from the east–west trending shelf break to the coast and is 500–600 m deep at its shallowest point near the shelf break (Fig. 1). The continental slope is comparatively steep, with a slope of 0.1 in the east and 0.05 farther west. Several West Antarctic Ice Sheet glaciers terminate on the inner (southern) shelf, where a number of 1500–2000-m-deep basins have formed. A 300-m ridge separates the deep basin in the eastern Amundsen shelf from the three shallower basins farther west.

Figure 2 shows temperature T and salinity S profiles seaward of the shelf break and in the basins on the shelf. The upper 200–400 m is dominated by a layer of fresh, cold Winter Water (WW), which is defined as having neutral density (Jackett and McDougall 1997) $\gamma_N < 28.03$ and temperature $T < -1.6°C$ (Bindoff et al. 2000). Below this, the CDW, which is defined as having

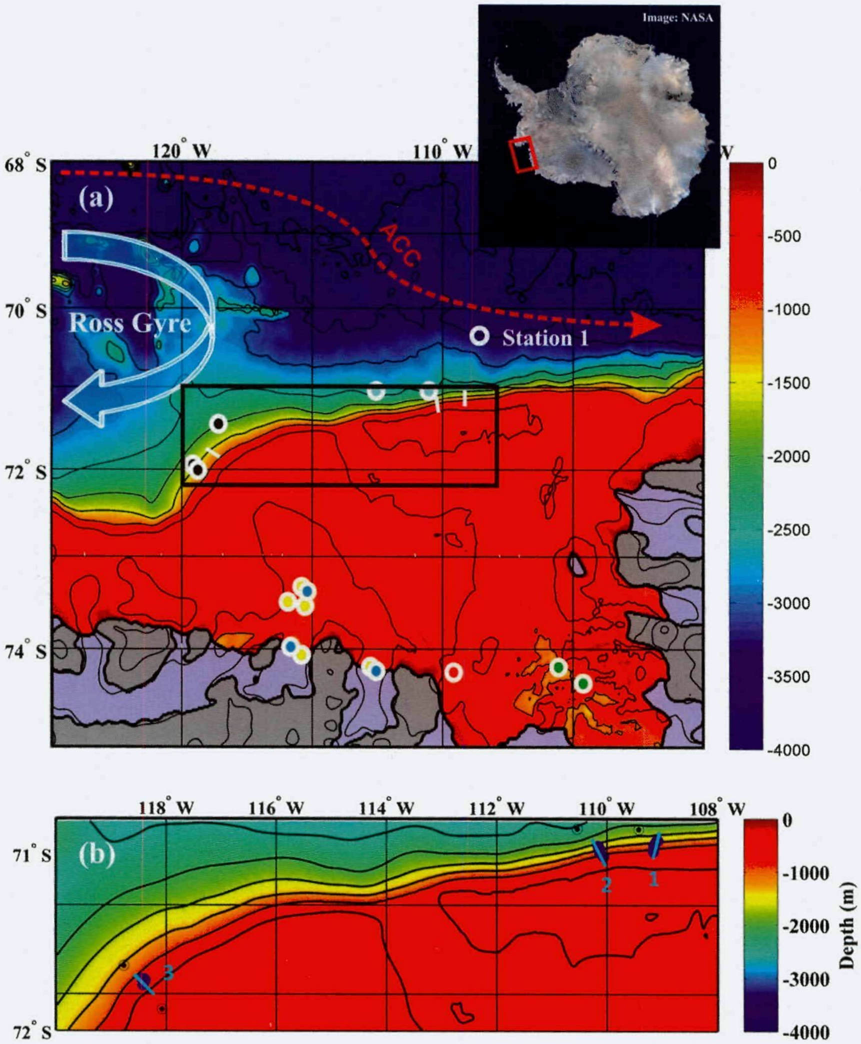

FIG. 1. Map of the region together with location of stations and the three sections studied here. Bathymetry from Timmermann et al. (2010). (a) Arrows indicate the Ross gyre and the southern extent of the ACC (after Orsi et al. 1995). Colored circled dots indicate the location of historical CTD stations in the inner basins and outside the shelf break. (b) Location of the three sections. Purple dots indicate CTD stations, and black circled dots indicate the off-shelf stations (occupied during the same cruise) that were used to extrapolate the section edges. Also shown is station 1, which is used as background reference station in section 3.

$28.27 > \gamma_N > 28.03$ (Whitworth et al. 1998), resides. At the off-shelf stations, the CDW is stratified and clearly shows the expected (e.g., Whitworth et al. 1998) temperature maximum. At the shelf stations, the layer of WW is thicker than at the off-shelf stations. The warm deep water is more homogeneous on the shelf and occupies the deep basins from sill depth (500–600 m) to the bottom. Between the WW and the unmodified CDW, there is a layer of modified CDW that has been mixed with ice shelf meltwater, characterized by the alignment along the Gade line (Gade 1979) in the T–S plane (Wåhlin et al. 2010). This mixture is only present at the shelf stations, as can be seen in the T–S diagram (Fig. 2c).

The shelf water is generally colder and less saline in the west than in the east. Basin water at 1000-m depth is about 0.3°C colder and 0.1 g kg^{-1} less saline and the WW layer is about 200 m thicker (Figs. 2a,b). It can be noted that the water on the shelf has warmed substantially over the past decade, particularly in the west. The stations marked with blue dots in the western basin (blue lines, Fig. 2) were occupied in 1994 and 2000 and show temperatures at 1000 m of ~0°C. The stations marked with yellow dots in Fig. 1 (yellow lines in Fig. 2) were

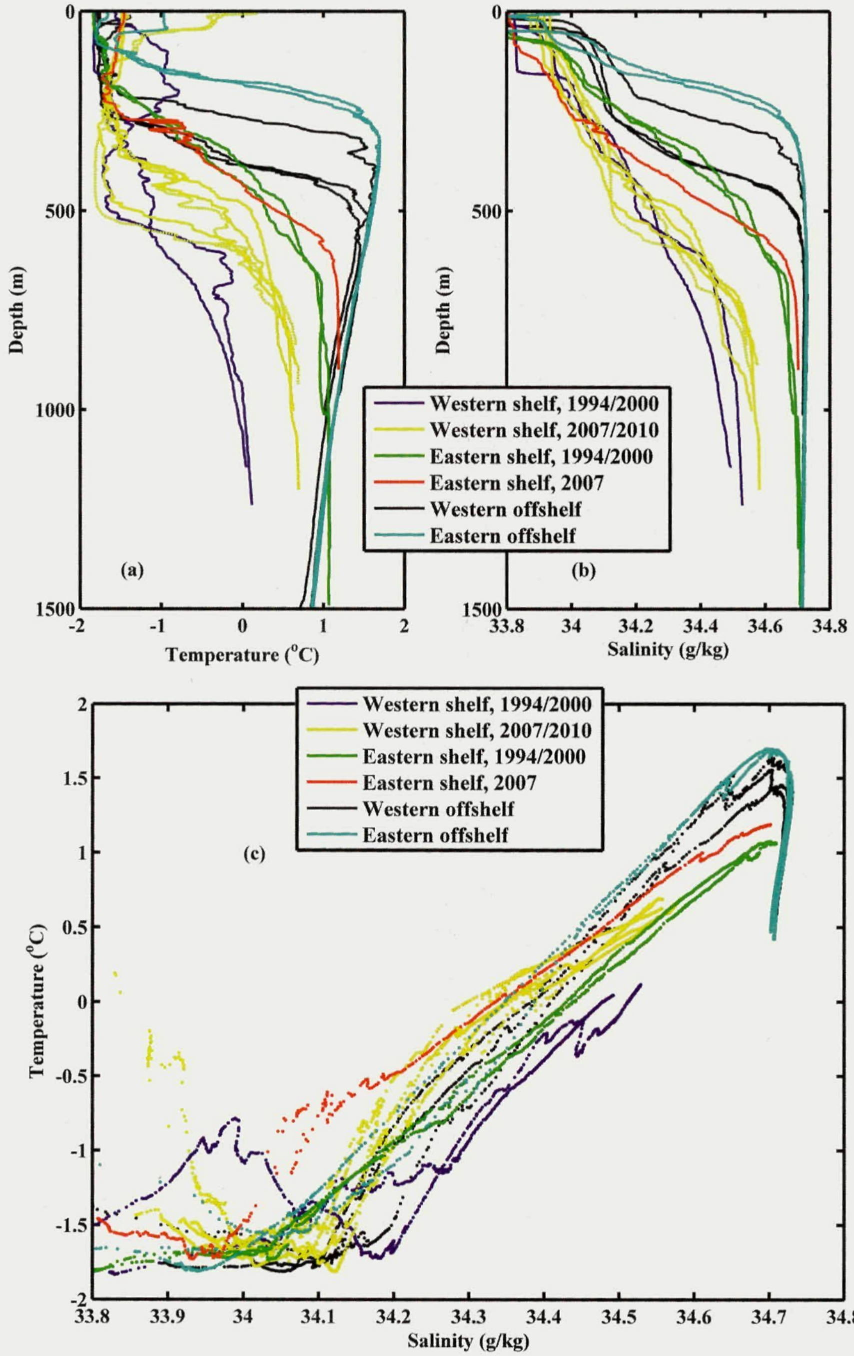

FIG. 2. Temperature and salinity for the historical stations shown in Fig. 1. Line colors correspond to station colors in Fig. 1 according to legend. Data from 1994 and 2000 were provided by NODC (Boyer et al. 2006); 2007 data from the *Oden* 2007 cruise (courtesy of X. Yuan and S. Stammerjohn 2012, personal communication), 2010 data from the *Araon* 2010 cruise. (a) Vertical plot of temperature, (b) vertical plot of salinity, and (c) temperature–salinity plot.

occupied during 2007 and 2010 and show T ~0.6°C at 1000 m. The same is true for the eastern basin, where Jacobs et al. (2011) noted a warming of 0.45° in the thermocline between 1994/2000 and 2007/09 (also detected here; cf. red and green profiles in Fig. 2a). T–S characteristics (Fig. 2c) for deep eastern basin water (from 700 m to the bottom) are similar to those of the Lower Circumpolar Deep Water: that is, T = 1°–1.2°C and

$S = 34.7$–34.72 g kg^{-1}, which can be found at 800–1000-m depth outside the shelf. Water with this T–S signature has been observed to flow toward the glaciers in the deep troughs leading to the eastern basin in 2004 (Walker et al. 2007) and in 2009 (Jacobs et al. 2011). The deep water in the western basins has temperature $T = 0.6$°C and salinity $S = 34.55$ g kg^{-1}, a strongly modified (compared to the eastern shelf) version of what can be found outside the shelf as is clear from the T–S diagram (Fig. 2c).

b. *Shelf break and upper slope structure*

The survey of the central Amundsen shelf in December 2008–January 2009 included transects extending from the outer shelf across the shelf break at sites in the eastern and western Amundsen Sea (Figs. 1b, 3). Hydrographic data were sampled using a Sea-Bird SBE 911+ CTD system with a dual sensor pack that included SBE 3+ temperature, SBE 4C conductivity, and SBE 43 oxygen sensors. The sensors were calibrated before and after the cruise and the data corrected for drift in salinity, temperature, and oxygen. Current shear was measured using a Teledyne RDI 300-kHz Workhorse Sentinel lowered acoustic Doppler current profiler (LADCP) attached to the CTD rosette sampler. Velocity data were detided using a 10-component barotropic tide model Circum-Antarctic Tidal Simulation, Inverse Model Version 2008a (CATS2008b; Padman et al. 2002), which has been shown to agree well with the tidal variability measured by LADCP in other locations of the Amundsen shelf (Wåhlin et al. 2010). Maximum tidal speeds ranged from 0.01 to 0.04 m s^{-1} and were at most locations small compared to the vertical average of the measured velocities.

Cross-slope sections show the distributions of temperature T, salinity S, oxygen (O_2), and the detided velocity components along and across the eastern and western Amundsen Sea transects (Fig. 3). The two easternmost sections (sections 1 and 2; Figs. 3a,b) are qualitatively similar to each other and show a roughly 1000-m-thick eastward flow along the slope with speeds around 0.2 m s^{-1}. The water was stratified with maximum $T \sim 1.6$°C and minimum $O_2 \sim 4$ ml l^{-1} at 400 m. Salinity had a maximum $S \sim 34.722$ g kg^{-1} near 700 m. Beneath the eastward current there was a ~150-m-thick bottom layer in which velocities were comparatively small and isolines for T, S, O_2, and density tilted upward toward the shelf break following the bottom contours.

Conditions along the western section (section 3) differed from those at sections 1 and 2 farther east. The along-slope current was westward rather than eastward, and the water in this current was colder ($T \sim 0.6$°C), more oxygen rich ($O_2 \sim 4.7$ ml^{-1}), and fresher ($S \sim 34.6$ g kg^{-1}) than in the eastern sections. An off-shelf flow of relatively dense, cold, and oxygen-rich bottom water took place in a marked benthic boundary layer, about 50 m thick (Fig. 3c). In similarity with the historical stations (Fig. 2), the layer of WW was deeper in the westernmost section, where it approached 400 m, similar to the eastern Ross Sea (Orsi and Wiederwohl 2009).

The baroclinic pressure gradient arising from the sloping isopycnals at the shelf break induces a baroclinic geostrophic velocity that was computed relative to the sea surface for the two easternmost sections (Fig. 4). In similarity with the LADCP measurements, the geostrophic velocity decreases in a layer 100–200 m above the bottom. The relative decrease is similar in magnitude for both the observed LADCP and the computed geostrophic velocities (this information will be used in section 3). For example, compare the profiles in Fig. 4c, where the LADCP velocity drops from 0.1 to 0 m s^{-1} between 800 and 1000 m and the geostrophic drops from 0 to -0.15 in the same depth interval, and in Fig. 4g, where the LADCP drops from 0.15 to -0.05 m s^{-1} from 400- to 600-m depth and the geostrophic drops from 0.5 to 0.35 m s^{-1}.

3. Boundary layer dynamics

When a barotropic current flows over a solid seabed in a rotating system, the induced stress gives rise to an Ekman transport $\mathbf{m}_E = (m_E^x, m_E^y)$ in the benthic boundary layer (Fig. 5). This transport is directed to the right of the overlying flow $\mathbf{U} = (U, V)$ in the Southern Hemisphere and increases with the speed of the barotropic current and the induced stress according to

$$m_E^Y = \delta_E U, \qquad (1)$$

where m_E^Y (m^2 s^{-1}) is the cross-shelf component per unit length of the Ekman transport $\mathbf{m}_E$ and δ_E is the Ekman layer thickness that can be parameterized in different ways (e.g., Wåhlin and Walin 2001). For a quadratic drag law, we use

$$\delta_E = C_D \frac{|\mathbf{U}|}{f}, \qquad (2)$$

where C_D is the quadratic bulk friction drag coefficient and f is the Coriolis parameter. Using values pertinent for the observations (i.e., $|\mathbf{U}| = 0.2\,\mathrm{m\,s^{-1}}$, $f = -1.38 \times 10^{-4}\,\mathrm{s^{-1}}$, and $3 \times 10^{-3} < C_D < 5 \times 10^{-3}$), we find that δ_E is between 4 and 7 m and m_E is between 0.9 and 1.4 m^2 s^{-1}. The Ekman transport takes place in a layer of approximate thickness $\pi\delta_E$ (see, e.g., Cossu et al. 2010): that is, 14–23 m, assuming the foregoing parameters. The maximum speed in the Ekman layer is about half that of the overlying current (see, e.g., Cossu

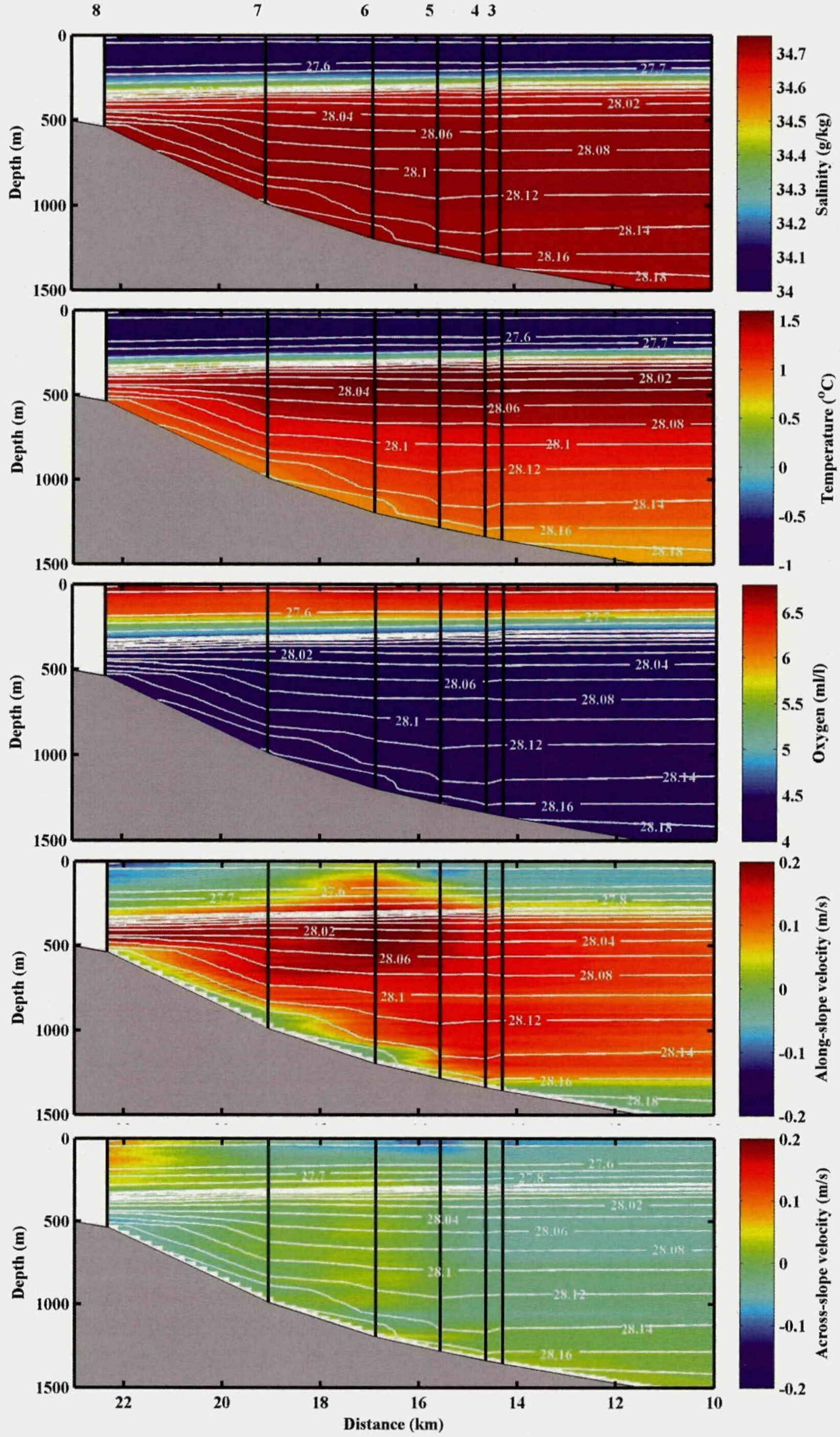

FIG. 3. Cross-slope sections of salinity (g kg^{-1}), temperature (°C), dissolved oxygen concentration (ml l^{-1}), and across- and along-slope currents (m s^{-1}) according to color bars. White lines represent contours of neutral density γ_N (Jackett and McDougall 1997). Data at the left and right edges of the sections are extrapolations toward the closest off-shelf and on-shelf stations, indicated by black circled dots in Fig. 1, occupied during the same cruise. (a) Section 1, (b) section 2, and (c) section 3. Section locations are shown in Fig. 1b; the contours were interpolated between the stations using cubic interpolation.

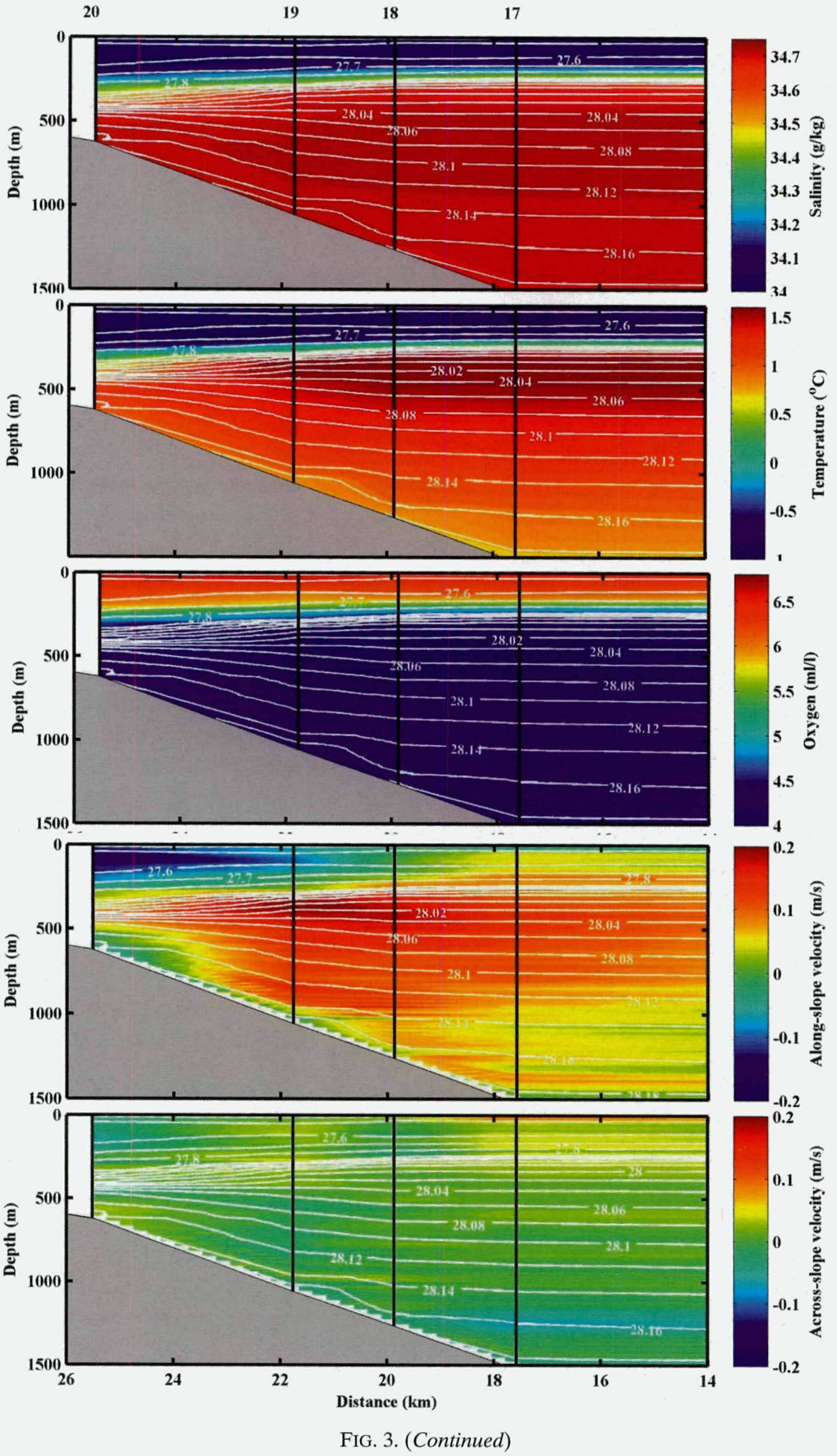

FIG. 3. (*Continued*)

et al. 2010): that is, 0.1 m s^{-1} in the present case. In section 3 (Fig. 3c), the LADCP recorded a westward flow of about 0.2 m s^{-1} that decreased to zero in a 40-m-deep layer near the seabed. A seaward cross-slope flow in this layer had a local velocity maximum of 0.1 m s^{-1} (Fig. 3c). Although the boundary layer thickness is somewhat larger than (2), the flow direction and speed in section 3 were essentially consistent with standard

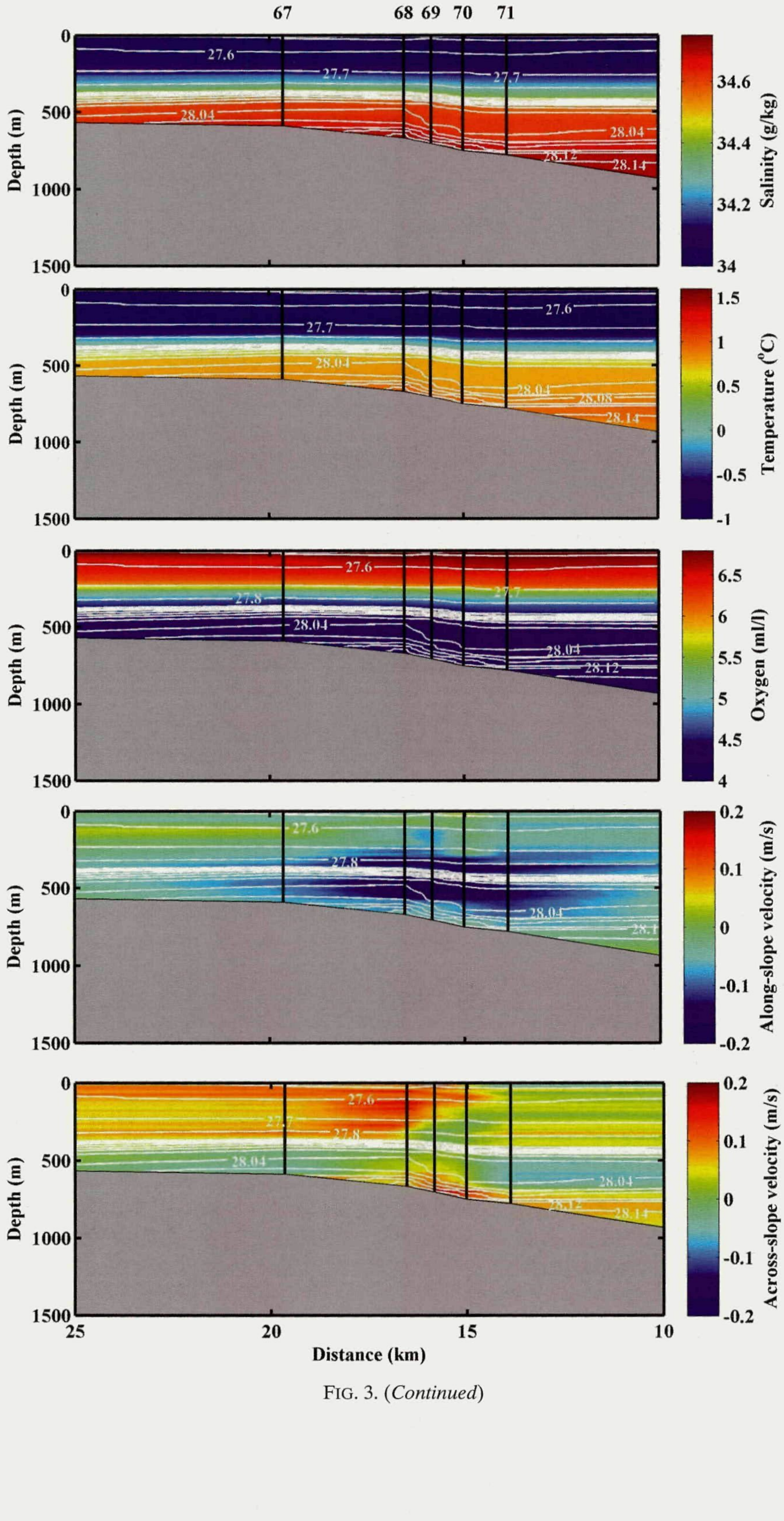

FIG. 3. (*Continued*)

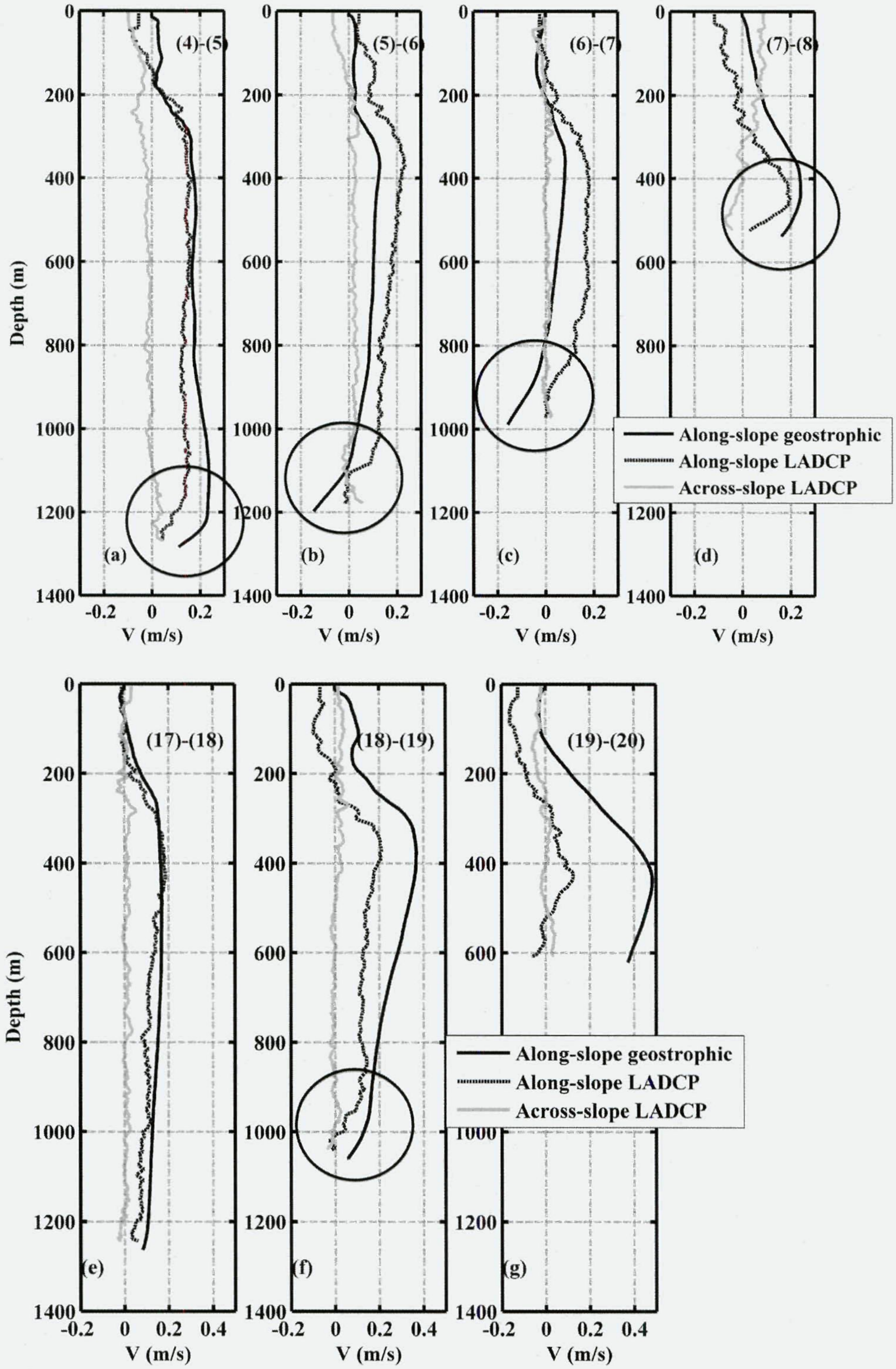

FIG. 4. Along-slope geostrophic velocities relative to the surface (solid); along-slope LADCP velocities (dashed); and across-slope LADCP velocities (dotted). (a)–(d) Section 1 and (e)–(g) section 2. Numbers refer to the stations between which the pressure gradients for the geostrophic shear were calculated (for location, see Fig. 3).

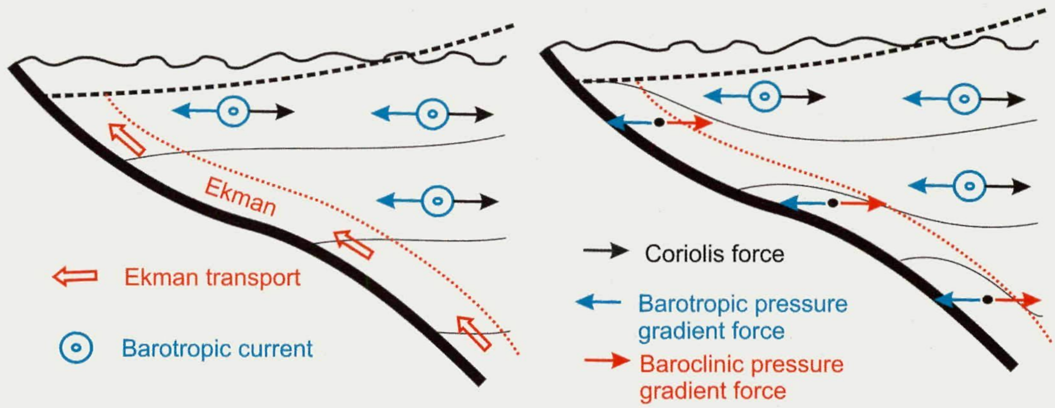

FIG. 5. Sketch of the barotropic velocity, induced Ekman transport, and lifting of isopycnals that lead to slippery Ekman layers. (left) The isopycnals (black thin lines) before lifting and (right) the isopycnals at steady state (i.e., when the baroclinic pressure gradient at the bottom balances the barotropic pressure gradient that drives the main flow).

Ekman theory [cf. Eqs. (1) and (2)]. The eastern sections, 1 and 2, are less compatible with standard Ekman theory. There is a bottom layer in which the along-slope speed decreases to zero, but the layer thickness is an order of magnitude larger than that expected from (2). The cross-slope velocity is close to zero throughout the water column, and there is no trace of the expected local velocity maximum in the bottom layer (Fig. 4).

When the fluid is vertically stratified and the bottom slopes, the Ekman transport will advect relatively dense fluid up (or down) the slope, which generates buoyancy forces close to the bottom (Fig. 5). These buoyancy forces are directed oppositely to the pressure gradient force driving the overlying barotropic flow. As long as the Ekman transport continues to transport water up (or down) the slope, the buoyancy forces will continue to grow. When they become sufficiently large, they can cancel out the interior pressure gradient. The net pressure gradient in the bottom boundary layer then becomes close to zero. As a consequence, the geostrophic velocity is greatly reduced, as are the frictional shear and the associated Ekman transport. When this happens, the Ekman layer is said to be arrested (MacCready and Rhines 1991; Trowbridge and Lentz 1991; MacCready and Rhines 1993; Garrett et al. 1993). The dynamics of arrested Ekman layers on sloping bottoms have been considered for the case of a buoyant coastal boundary current (Trowbridge and Lentz 1991), for a barotropic jet in a stratified ocean (MacCready and Rhines 1991; MacCready and Rhines 1993; Garrett et al. 1993), and for a dense current beneath a stagnant homogeneous water mass (Wåhlin and Walin 2001). In each of these cases, the density and velocity fields evolve to a state in which the net pressure gradient close to the bottom, and hence the geostrophic velocity there, is zero. Because the along-slope velocity is zero, the Ekman transport also becomes zero. The phenomenon has also been referred to as "slippery Ekman layers" (MacCready and Rhines 1993). Arrested Ekman layers in the Southern Hemisphere are associated with shoreward lifting of the isopycnals and zero bottom velocity (Fig. 5), for flow directed with the coast to the right (eastward for the Amundsen Sea).

In sections 1 and 2, there was during the time of measurements a strong eastward current in the water column down to within 150–200 m of the bottom (Figs. 3, 4). Furthermore, T, S, and O_2 isolines were lifted shoreward along the bottom, indicating that water had been transported up the slope from greater depths. The upslope velocity in the bottom layer was, however, much smaller than that predicted by Ekman theory (Figs. 3, 4). These findings suggest that the Ekman layer could have become arrested. A more quantitative estimate of whether the Ekman layer is arrested can be obtained by comparing the geostrophic and the LADCP velocity profiles (Fig. 4). The average speed in the interior water column was around 0.2 m s^{-1} as measured by the LADCP (Figs. 3, 4). In section 1 the geostrophic velocities decrease by about 0.2 m s^{-1} in the bottom 150–200 m, a consequence of the fact that dense water from deeper down has been shifted upslope, creating a countering buoyancy force. The fact that the calculated geostrophic velocity reduction in the bottom layer is approximately equal to the measured velocity outside the bottom layer requires that the baroclinic pressure gradient in the bottom layer and the barotropic pressure gradient outside the boundary layer are approximately equal in magnitude (i.e., pressure compensation). Further, the vertical shear in the bottom 200 m is similar for the LADCP and the geostrophic velocities in section 1, consistent with a thermal wind balance bringing the velocity to zero rather than frictional stress. Pressure compensation is also evident in the shallower stations of section 2, but not in the deeper ones, where the along-slope LADCP velocity was smaller and the lifting of the isolines was less evident (Figs. 3, 4).

The time scale for Ekman layers to become arrested is approximately given by (MacCready and Rhines 1991, 1993)

$$\tau_0 = \frac{f}{(N\alpha)^2}, \tag{3}$$

where N (s^{-1}) is the buoyancy frequency and α is the slope of the bottom. Using values pertinent for the present observations (i.e., $f = 1.38 \times 10^{-4}\ s^{-1}$, $N = 1.2 \times 10^{-3}\ s^{-1}$, and $\alpha = 0.1$), we get $\tau_0 \approx 4$ h. This means that it takes approximately 4 h for the Ekman transport to move dense water sufficiently far up the slope so that the Ekman layer becomes arrested. Because there is pressure compensation next to the seabed, at least in section 1, this indicates that the presently observed along-shelf flow has been going on for at least 4 h. The thickness of the boundary layer in arrested Ekman dynamics increases with time, and for times larger than τ_0 the thickness is large compared to (2) (MacCready and Rhines 1991). This is consistent with the observed boundary layer thickness (Figs. 3, 4) of over 150 m.

In a steady state [i.e., when isopycnal slopes in the bottom layer equal the seabed slope (as in Fig. 3) and the baroclinic pressure gradient precisely balances the barotropic], the density difference between the uplifted water and undisturbed water farther off shelf should be such that (MacCready and Rhines 1993)

$$g'\alpha = fU, \tag{4}$$

where $g' = g(\Delta\rho/\rho_0)$ is the reduced gravity and $\Delta\rho(z) = \rho_{UD}(z) - \rho_L(z)$ is the density difference between the undisturbed water at level z (ρ_{UD}) and the uplifted water (ρ_L). From (4), the density difference at the shelf break can be obtained as

$$\Delta\rho = fU\frac{\rho_0}{g\alpha}, \tag{5}$$

which (using $f = -1.38 \cdot 10^{-4}\ s^{-1}$, $\alpha = 0.1$, and $U = 0.2\ m\ s^{-1}$) gives $\Delta\rho = 0.03\ kg\ m^{-3}$, comparable to the 0.03–0.04 kg m^{-3} seen in Fig. 3.

When Ekman layers become arrested, the associated transport approaches a steady value that is much smaller than the Ekman transport (MacCready and Rhines 1993). However, at the shelf inland of the shelf break, the bottom is horizontal and it is not possible for the Ekman layer to be arrested. Where the bottom is horizontal, the relatively dense water that has been transported up from greater depths can flow south toward the coast (Jacobs et al. 2011). Because this dense water is constantly removed from near the shelf break by the southward flow, the transport in the arrested bottom layer never actually shuts down. It does, however, take place in a layer much thicker than the Ekman layer (MacCready and Rhines 1993), in which the thermal wind balance rather than friction brings the velocity to zero. Because the flow is spread out in a layer that is an order of magnitude thicker than the Ekman layer, the velocities are expected to be comparatively small, consistent with the data (Figs. 3, 4).

Figure 6 shows the vertical variation of neutral density γ_N (Jackett and McDougall 1997), S, T, and O_2 content for station 1, located off the shelf at around 2000-m depth (Fig. 1a). Also shown is the range of values for the three additional off-shelf stations that were occupied during the cruise (circled dots, Fig. 1b). Assuming this profile to be representative for the off-shelf water, a density difference $\Delta\rho = 0.03\ kg\ m^{-3}$ [cf. (5)] would mean that water at the shelf break (~600-m depth) would be withdrawn from slope waters ~900 m deep. Such water has S = 34.7 psu, T = 1°–1.2°C, and $O_2 \approx 4.3$ ml l^{-1}. The eastern basin is presently filled with water whose T–S properties (Fig. 2) suggest that inflow of water originating at 900-m depth off shelf is a regular occurrence. Because 900 m is also the withdrawal depth predicted by (5), the present results are not incompatible with the idea that filaments of the ACC may venture close to the shelf break in the eastern part of the Amundsen shelf and then induce cross-shelf transport of warm CDW onto the shelf. The scenario seems less likely to occur frequently on the western part of the region, where no unmodified water originating off shelf was found.

4. Discussion and conclusions

The new observations presented here show a strong eastward flow in the eastern shelf and upward-sloping isolines of T, S, and O_2 paralleling the bottom. The sloping isolines are indicative of an upward transport of water from greater depths in the bottom layer, although the shoreward velocity in the bottom layer was close to zero at the time of measurement. The vertical variation of the along-slope (eastward) velocity and density field was consistent with a thermal wind balance bringing the velocity to zero in the bottom layer, rather than friction. This is in accordance with the theory of arrested Ekman layers (e.g., MacCready and Rhines 1991; Trowbridge and Lentz 1991). Water in the eastern shelf basin has the

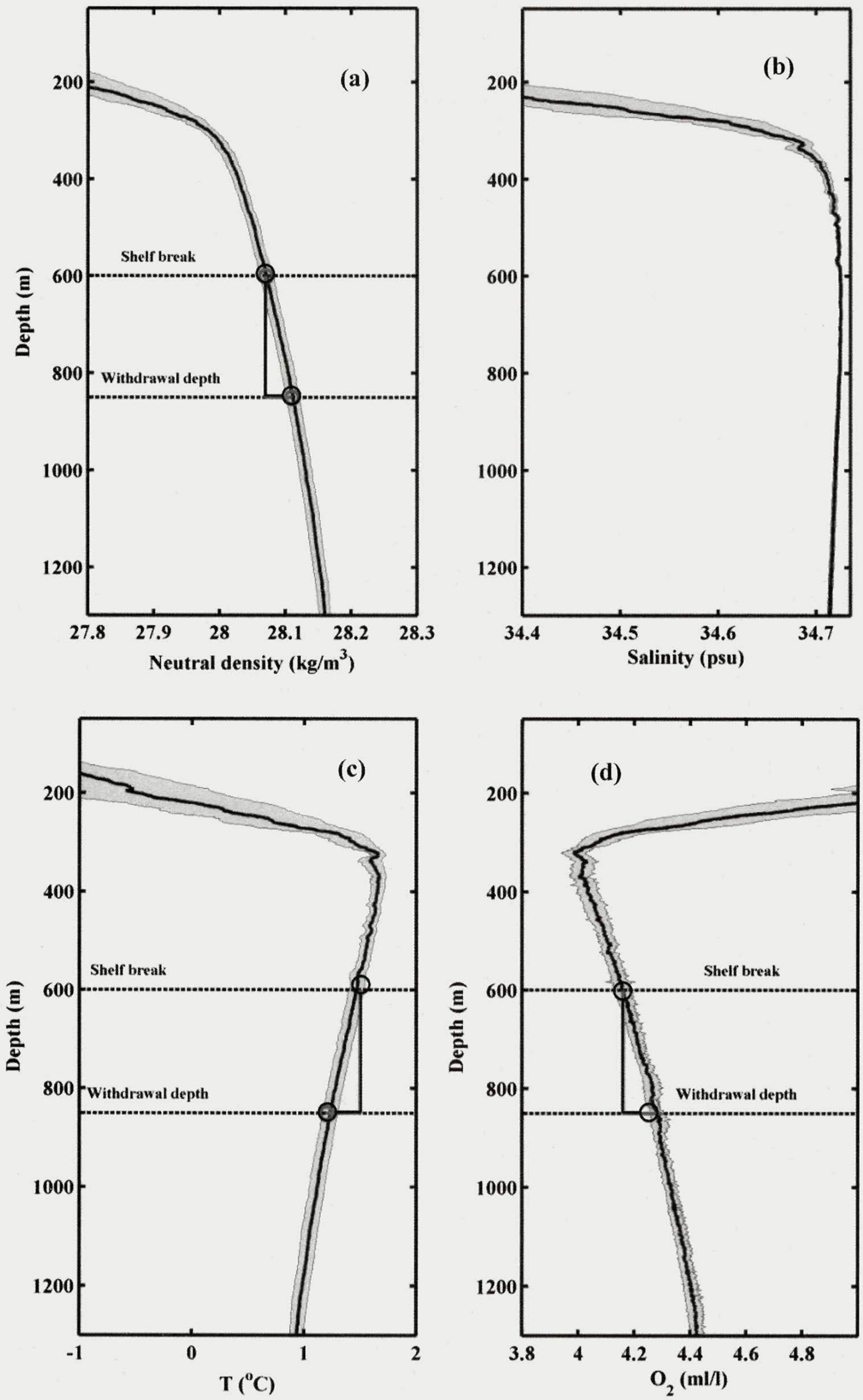

FIG. 6. Background profiles of (a) neutral density γ_N, (b) salinity, (c) temperature, and (d) oxygen, with reference lines inserted for the shelf break and withdrawal depth for sections 1 and 2.

same T–S properties as water at 800–1000-m depth off shelf, indicating that transport of off-shelf water from this depth onto the shelf regularly takes place. Available data are inadequate to determine how frequently this situation occurs or how important Ekman dynamics is for the time mean on-shelf flow of Circumpolar Deep Water. In general, we anticipate significant time variability in Amundsen Sea slope currents. This anticipation is based in part on potential forcing by the off-shelf ACC, which near the shelf break has broken up into a complex band of eddies and filaments (K. Dohan 2011, personal communication). Additionally, we can expect variations in surface forcing due to wind and ice cover variability.

At the time of the cruise a strong westward flow and a northward near-bottom transport were observed in the western part of the shelf. However, this is clearly not always the case because the water in the basin is warmer than the WW and must have originated outside the shelf before mixing (Fig. 2c). Furthermore, a 0.3–0.4-Sv (1 Sv ≡ 10^6 m^3 s^{-1}) southward flow of 1°C water was observed in the western trough only a week prior to the present observations (Wåhlin et al. 2010). Recent observations from a mooring in the western trough show that there is large temporal variability of the velocity but that nearly all the variance lies in the barotropic mode (L. Arneborg et al. 2012, unpublished manuscript). The 0.6°C water in the western inner shelf is significantly less saline than the 0.6°C off-shelf water. Assuming the shelf water to be derived in part from off-shelf water, it must have been subject to mixing with some other water mass: for example, ice shelf meltwater from subsurface melting processes. The mechanism for the net flow of warm salty water into the western basin thus remains unclear; the present results indicate that it is likely not forced by Ekman dynamics coupled to the ACC.

The present observations suggest that the bifurcation point between the ACC and the Ross gyre falls somewhere in between 120° and 110°W. Eastward flow along the shelf was observed at 110°W, and westward flow was observed at 118°W. Ekman transport induced by a barotropic eastward current east of 115°W would pump warm deep water into the troughs, leading to the eastern shelf basins (Fig. 1), which could explain the presence of such water there. If eastward flow west of 115°W would occur, Ekman dynamics would pump water into the western shelf basin, where no warm water originating off shelf was found. The mechanism of arrested Ekman layers in combination with the location of the bifurcation point presents a possible explanation of the observed difference in basin water properties between the eastern and western shelf basins.

The results presented here are consistent with the presence of Ekman induced on-shelf transport along the eastern Amundsen Sea shelf break at the time of data collection. It is hypothesized that this could happen at other occasions too and that the mechanism might contribute significantly to the cross-shelf transport of warm water onto the shelf. Assuming that the ACC was to impinge on the entire eastern shelf break (approximately 300 km long), the net induced shoreward transport can be estimated using (1). With $U = 0.2\,\mathrm{m\,s^{-1}}$, $f = -1.38 \times 10^{-4}\,\mathrm{s^{-1}}$, and $C_D = 3 \times 10^{-3}$, the transport is $0.9\,\mathrm{m^2\,s^{-1}} \times 300\,\mathrm{km} = 0.25\,\mathrm{Sv}$, comparable in magnitude to the 0.26-Sv inflow through the eastern trough reported by Walker et al. (2007). This estimate suggests that Ekman transport driven by ACC filaments impinging on the shelf break could contribute significantly to flow of CDW onto the eastern Amundsen shelf. As a final caveat, we note that our hypothesis assumes, lacking detailed bathymetric information, an absence of small-scale bathymetric features that might impact local dynamics (e.g., Allen and de Madron 2009) and our transport estimates.

Acknowledgments. The cruise *Oden* Southern Ocean 2008/09 was carried out on IB *Oden*, and we are grateful for help and logistic support from the captain and crew. Bengt Liljebladh, Kevin Pedigo, and Jeremy Lucke provided expert technical assistance with preparations as well as during the cruise. The cruise was supported by National Science Foundation (NSF), Swedish Polar Research Secretariat, and the Swedish Research Council (SRC). We are grateful to Sharon Stammerjohn and Xiaoyun Yuan for providing comments on the manuscript and data from the *Oden* 2007 cruise. The data from the World Ocean Database were compiled by the National Oceanographic Data Center of NOAA. Wåhlin was funded by SRC (Grants 824-2008-6439 and 2010-19172-73868-33) and Vinnova, Björk was funded by SRC (Grant 824-2008-6439), Arneborg was funded by SRC (Grant 621-2008-2689), and Muench was funded by NSF through NSF Grants OPP-0125602 and ANT-0440656 and ONR Grant N00014-03-1-0067 to Earth & Space Research. Ha and Lee were supported by KOPRI Grant PE11040.

REFERENCES

Allen, S., and X. D. de Madron, 2009: A review of the role of submarine canyons in deep-ocean exchange with the shelf. *Ocean Sci.*, **5**, 607–620.

Beardsley, R. C., R. Limeburner, and W. B. Owens, 2004: Drifter measurements of surface currents near Marguerite Bay on the western Antarctic Peninsula shelf during austral summer and fall, 2001 and 2002. *Deep-Sea Res. II*, **51**, 1947–1964, doi:10.1016/j.dsr2.2004.07.031.

Bindoff, N. L., M. A. Rosenberg, and M. J. Warner, 2000: On the circulation and water masses over the Antarctic continental slope and rise between 80 and 150°E. *Deep-Sea Res. II,* **47,** 2299–2326.

Boyer, T. P., and Coauthors, 2006: *World Ocean Database 2005.* NOAA Atlas NESDIS 60, 190 pp.

Cossu, R., M. G. Wells, and A. K. Wåhlin, 2010: Influence of the Coriolis force on the velocity structure of gravity currents in straight submarine channel systems. *J. Geophys. Res.,* **115,** C11016, doi:10.1029/2010JC006208.

Dinniman, M. S., and J. M. Klinck, 2004: A model study of circulation and cross-shelf exchange on the west Antarctic Peninsula continental shelf. *Deep-Sea Res. II,* **51,** 2003–2022, doi:10.1016/j.dsr2.2004.07.030.

Foldvik, A., and Coauthors, 2004: Ice shelf water overflow and bottom water formation in the southern Weddell Sea. *J. Geophys. Res.,* **109,** C02015, doi:10.1029/2003JC002008.

Gade, H., 1979: Melting of ice in sea water: A primitive model with application to the antarctic ice shelf and icebergs. *J. Phys. Oceanogr.,* **9,** 189–198.

Garrett, C., P. MacCready, and P. Rhines, 1993: Boundary mixing and arrested Ekman layers: Rotating stratified flow near a sloping boundary. *Annu. Rev. Fluid Mech.,* **25,** 291–323, doi:10.1146/annurev.fl.25.010193.001451.

Gordon, A. L., E. Zambianchi, A. Orsi, M. Visbeck, C. Giulivi, T. Whitworth III, and G. Spezie, 2004: Energetic plumes over the western Ross Sea continental slope. *Geophys. Res. Lett.,* **31,** L21302, doi:10.1029/2004GL020785.

——, A. H. Orsi, R. Muench, B. A. Huber, E. Zambianchi, and M. Visbeck, 2009: Western Ross Sea continental slope gravity currents. *Deep-Sea Res. II,* **56,** 796–817.

Hofmann, E. E., P. H. Wiebe, D. P. Costa, and J. J. Torres, 2004: An overview of the Southern Ocean Global Ocean Ecosystems Dynamics program. *Deep-Sea Res. II,* **51,** 1921–1924, doi:10.1016/j.dsr2.2004.08.007.

Jackett, D. R., and T. R. McDougall, 1997: A Neutral Density Variable for the World's Oceans. *J. Phys. Oceanogr.,* **27,** 237–263.

Jacobs, S., A. Jenkins, C. Giulivi, and P. Dutrieux, 2011: Stronger ocean circulation and increased melting under Pine Island Glacier ice shelf. *Nat. Geosci.,* **4,** 519–523.

Jenkins, A., P. Dutrieux, S. S. Jacobs, S. D. McPhail, J. R. Perrett, A. T. Webb, and D. White, 2010: Observations beneath Pine Island Glacier in West Antarctica and implications for its retreat. *Nat. Geosci.,* **3,** 468–472, doi:10.1038/ngeo890.

Klinck, J. M., and M. S. Dinniman, 2010: Exchange across the shelf break at high southern latitudes. *Ocean Sci.,* **6,** 513–524, doi:10.5194/os-6-513-2010.

——, E. E. Hofmann, R. C. Beardsley, B. Salihoglu, and S. Howard, 2004: Water-mass properties and circulation on the west Antarctic Peninsula continental shelf in austral fall and winter 2001. *Deep-Sea Res. II,* **51,** 1925–1946, doi:10.1016/j.dsr2.2004.08.001.

MacCready, P., and P. B. Rhines, 1991: Buoyant inhibition of Ekman transport on a slope and its effect on stratified spin-up. *J. Fluid Mech.,* **223,** 631–666.

——, and ——, 1993: Slippery bottom boundary layers on a slope. *J. Phys. Oceanogr.,* **23,** 5–22.

Orsi, A., and C. Wiederwohl, 2009: A recount of Ross Sea Waters. *Deep-Sea Res. II,* **56** (13–14), 778–795.

——, T. Whitworth, and W. Nowlin, 1995: On the meridional extent and fronts of the Antarctic Circumpolar Current. *Deep-Sea Res. I,* **42,** 641–673.

Padman, L., H. A. Fricker, R. Coleman, S. Howard, and S. Erofeeva, 2002: A new tide model for the Antarctic ice shelves and seas. *Ann. Glaciol.,* **34,** 247–254.

Rignot, E., 1998: Fast recession of a West Antarctic glacier. *Science,* **281,** 549–551.

——, and S. Jacobs, 2002: Rapid bottom melting widespread near Antarctic ice sheet grounding lines. *Science,* **296,** 2020–2023.

Shepherd, A., D. Wingham, and E. Rignot, 2004: Warm ocean is eroding West Antarctic Ice Sheet. *Geophys. Res. Lett.,* **31,** L23402, doi:10.1029/2004GL021106.

Thoma, M., A. Jenkins, D. Holland, and S. Jacobs, 2008: Modelling Circumpolar Deep Water intrusions on the Amundsen Sea continental shelf, Antarctica. *Geophys. Res. Lett.,* **35,** L18602, doi:10.1029/2008GL034939.

Timmermann, R., and Coauthors, 2010: A consistent dataset of Antarctic ice sheet topography, cavity geometry, and global bathymetry. *Earth Syst. Sci. Data,* **2,** 261–273, doi:10.5194/essd-2-261-2010.

Trowbridge, J. H., and S. J. Lentz, 1991: Asymmetric behavior of an oceanic boundary layer above a sloping bottom. *J. Phys. Oceanogr.,* **21,** 1171–1185.

Wåhlin, A. K., and G. Walin, 2001: Downward migration of dense bottom currents. *Environ. Fluid Mech.,* **1,** 257–279.

——, X. Yuan, G. Björk, and C. Nohr, 2010: Inflow of warm Circumpolar Deep Water in the central Amundsen shelf. *J. Phys. Oceanogr.,* **40,** 1427–1434.

Walker, D. P., M. A. Brandon, A. Jenkins, J. T. Allen, J. A. Dowdeswell, and J. Evans, 2007: Oceanic heat transport onto the Amundsen Sea shelf through a submarine glacial trough. *Geophys. Res. Lett.,* **34,** L02602, doi:10.1029/2006GL028154.

Whitworth, T., III, A. H. Orsi, S.-J. Kim, and W. D. Nowlin Jr., 1998. Water masses and mixing near the Antarctic Slope Front. *Ocean, Ice, and Atmosphere: Interactions at the Antarctic Continental Margin,* S. S. Jacobs and R. F. Weiss, Eds., Antarctic Research Series, Amer. Geophys. Union, 1–27.